Chinese Journal of Polymer Science Vol. 35, No. 11, (2017), 1402−1414

Chinese Journal of Polymer Science
© Chinese Chemical Society
Institute of Chemistry, CAS
Springer-Verlag GmbH Germany 2017

Crystallization Kinetics and the Fine Morphological Evolution of Poly(ethylene oxide)/Ionic Liquid Mixtures*

Wen-ze Li, Yan-hua Niu**, Chen-ting Zhou, Huan Luo and Guang-xian Li
College of Polymer Science and Engineering, State Key Laboratory of Polymer Materials Engineering of China, Sichuan University, Chengdu 610065, China

Abstract The overall crystallization kinetics and spherulite morphologies of miscible poly(ethylene oxide) (PEO)/1-butyl-3-methylimidazolium hexafluorophosphate ([BMIM][PF_6]) mixtures were studied by differential scanning calorimetry (DSC), polarized optical microscopy (POM) and rheological measurements. The finer crystal structures were further detected by wide angle X-ray diffraction (WAXD) and small angle X-ray scattering (SAXS). Crystallization of PEO is largely suppressed by [BMIM][PF_6] addition especially at higher ionic liquid (IL) concentrations above 20 wt%. Both the overall crystallization rate and the spherulite growth decrease with the increase of IL content and crystallization temperature; however, the crystallization mechanism keeps unchanged as evidenced by the similar Avrami exponent n and WAXD results. The addition of [BMIM][PF_6] could induce more nuclei to some extent, but the induction time of crystallization is evidently prolonged, and a linear to non-linear transition of the spherulite growth ($R \propto t$ to $R \propto t^{1/2}$) can be observed. At higher IL concentration, the spherulite texture changes apparently from particular serrated to branch surface due to the diffusion-controlled growth and the dilution effect, which also as a main factor contributes to the increasing trend of the long period of crystals.

Keywords PEO; [BMIM][PF_6]; Crystallization kinetics; Spherulite morphologies

INTRODUCTION

There is extensive research toward the aim of achieving truly solid polymer electrolytes for applications in batteries and next-generation capacitors[1−4]. Poly(ethylene oxide) (PEO) as a polar polymer has been first found to be used in polymer electrolytes with high ionic conductivity when complexed with alkali metal salts[5]. In most polymer electrolytes, it is recognized that the amorphous phase alone rather than the initially assumed crystalline phase gives rise to ion transport[6]. Incorporation of lithium salts into the polymer matrix could significantly improve the ionic conductivity of polymer electrolytes by facilitating the amorphicity or suppressing crystallization[7−10]. However, how the crystallization kinetics and the resultant microstructure of polymer matrix influence the ion transport is still not well understood. Therefore, deeply understanding on the crystallization behaviors of polymers *i.e.* PEO with the secondary components in electrolyte materials and intentionally optimizing their performances are of great significance.

During the past years, a large amount of work has been focused on the miscibility and crystallization of PEO-based blends. It was reported that the addition of some lithium salts and other amorphous polymers could remarkably reduce the chain mobility of PEO and increase the glass transition temperature (T_g), which as a consequence leads to the decreased melting point and inhibited spherulite growth of PEO matrix[11, 12]. In addition, doping components with strong intermolecular interactions such as styrene and hydroxystyrene

* This work was financially supported by the National Natural Science Foundation of China (Nos. 51573115 and 51421061).
** Corresponding author: Yan-hua Niu (牛艳华), E-mail: yhniu@scu.edu.cn
Received March 6, 2017; Revised May 27, 2017; Accepted June 16, 2017
doi: 10.1007/s10118-017-1997-3

(SHS)[13], poly(acrylic acid) (PAA)[9, 14] into PEO could also largely suppress the PEO crystallization and strengthen the microphase separation. In recent years, more attention has been paid on ionic liquids (ILs) as either solvents for lithium salts or plasticizers for polymer-based electrolytes[15–17], due to their remarkable properties such as non- or low volatility, good chemical and thermal stability, and more importantly, the designable molecular structures and high ionic conductivity[18]. There is now growing interest in the new material design by tuning the microstructures and phase transitions of polymer/IL combinations, which provides potential applications in lithium ion batteries[19], fuel cells[20], and solar batteries[21] *etc.*

Recent publications have reported that PEO and its derivatives exhibit LCST (lower critical solution temperature) phase separation behavior in some imidazolium-based ILs driven by the specific interactions[22, 23]. In our previous work[24], the unique rheological and phase transition behaviors of PEO/1-alkyl-3-methylimidazolium tetrafluoroborate ([C$_n$MIM][BF$_4$]) mixtures have been investigated, in which the simultaneous occurrence of hydrogen bonding breaking and phase separating and their competition were found and identified for the first time. Besides the phase transition of such partially miscible polymer/ILs blends, there are relatively few studies paying attention to the crystallization behaviors of miscible PEO/IL mixtures[25–29]. Limited results show that the presence of 1-butyl-3-methylimidazolium hexafluorophosphate ([BMIM][PF$_6$]) could significantly inhibit the crystallization and spherulite growth of PEO matrix for either isothermal or non-isothermal process[28]. By changing the ILs structure, the strong interactions between PEO and ILs can be tuned, which was considered as a main factor contributing to the melting point (T_m) depression of PEO, that is, the stronger the molecular interaction, the more prominent T_m depression can be expected[25]. In these limited previous works, however, influences of IL itself and the resultant specific interactions *i.e.* hydrogen bonding between PEO and ILs on the polymer chain dynamics, crystallization kinetics more specifically the finer crystal microstructures, and even the ion transport still remain unclear. Therefore, deeper understanding on the crystallization behavior and complicated molecular interaction of PEO/ILs mixtures is imperative, which could provide potential guidance on the new electrolyte material design.

In this study, miscible PEO/[BMIM][PF$_6$] mixtures are selected as a model system to investigate the effect of IL addition on the crystallization behavior of PEO. Non-isothermal and isothermal crystallization of PEO/[BMIM][PF$_6$] at different IL concentrations under various crystallization temperatures were studied by DSC, optical microscopy and X-ray scattering techniques. High temperature crystallization was also monitored by rheological measurements, which have been proved to possess higher sensitivity compared to the DSC method at relatively lower crystallinity. The suppression of PEO crystallization with the addition of [BMIM][PF$_6$] is found, and the fantastic morphological evolution of PEO spherulites with coarsen textures especially at the later stages is presented for the first time. The changes from linear to non-linear spherulite growth during the whole crystallization process are also discussed. SAXS and WAXD results provide new evidences to understand the crystallization behavior of PEO/IL mixtures from lamellar scale. Therefore, this work is expected to shed some new lights on both the theoretical study of crystallization in polymer/ILs system and applications of new materials such as ion gels and polymer electrolytes.

EXPERIMENTAL

Materials and Sample Preparation

PEO was purchased from Sigma-Aldrich and used without further purification. The weight-average molecular weight (M_w) and the polydispersity index (PDI = M_w/M_n) were 1.25×10^5 g/mol and 1.63, respectively, which were determined by GPC measurements with monodisperse polystyrene as the standard and THF as the eluent phase at 30 °C. Ionic liquid [BMIM][PF$_6$] with purity ≥ 99% was purchased from Chengjie Shanghai.

PEO was first dissolved in dichloromethane at 40 °C with continuous stirring for at least 2 h, and then different amounts of [BMIM][PF$_6$] were added into the prepared solution with further stirring for at least 4 h until a homogeneous solution was obtained. The redundant solvent was removed by rotary evaporator at 40 °C. The prepared PEO/[BMIM][PF$_6$] mixtures with different PEO concentrations ranging from 50 wt% to 100 wt% were further dried at 40 °C for 24 h and stored in glove box to prevent moisture uptake. For clarification, the

sample codes with P95, P90, P80, P70, P60 and P50 were used in the latter sections, in which "P" stands for PEO and the number is PEO concentration.

Differential Scanning Calorimetry (DSC)

Thermal analysis was performed using a TA Instruments DSC Q20 with a Universal Analysis 2000. In the non-isothermal procedure, the samples were firstly heated to 107 °C for 5 min to eliminate any thermal history and subsequently cooled to –20 °C at the cooling rate of 10 K/min, after which the sample was heated to 107 °C for the second time at the same heating rate of 10 K/min. During isothermal crystallization, the samples were first annealed at 107 °C for 5 min, and then cooled to the target crystallization temperatures (T_{c1} = 43, 45, 47, 49 °C) at the cooling rate of 30 K/min. The samples with lower PEO concentrations of P70, P60 and P50 were not included in this process because of their rather lower crystallization temperatures.

Rheology

Rheological measurements were carried out using a TA instruments DHR-3 stress-controlled Rheometer with the parallel plates of 25 mm in diameter. The chosen gap was ~900 μm for all measurements. Dynamic time sweeps were performed with a fixed frequency of 1.0 rad/s and a given strain of 0.05% at the crystallization temperature of 52 °C for pure PEO, P95, P90 and P80 samples. Before the experimental running, the samples were first annealed at 107 °C for 5 min to eliminate thermal history. All rheological experiments were conducted in a nitrogen atmosphere. The disk samples with 25 mm in diameter and 1 mm in thickness were hot-pressed at 70 °C for use.

Polarized Optical Microscopy (POM)

The spherulite growth was observed by using an Olympus (BX61) optical microscope, equipped with a hot-stage and a temperature controller (Linkam CSS450). The samples were first annealed at 107 °C for 5 min, and then cooled to the crystallization temperatures at 30 K/min before observation. All samples for use were sandwiched between two pieces of glasses with a thickness of approximately 40 μm.

SAXS and WAXD

Small angle X-ray scattering (SAXS) experiments were performed in-house using a XENOCS instrument equipped with the GeniX^{3D} beam delivery system. The wavelength of the X-ray beam (Cu Kα) was 1.54 Å with the sample-to-detector distance about 2500 mm for SAXS and 140 mm for WAXD. The samples were sandwiched between two Kapton sheets with 1.0 mm in thickness in a hot-stage (Linkam HFX350) and isothermally crystallized for sufficient time at 49 °C after elimination of thermal history. All SAXS and WAXD experiments were conducted in a vacuum environment.

RESULTS AND DISCUSSION

Non-isothermal Melting and Crystallization Behaviors

As shown in Fig. 1, the DSC cooling and heating scan curves for PEO/[BMIM][PF_6] mixtures with different PEO contents ranging from 50 wt% to 100 wt% are reordered. Upon increasing [BMIM][PF_6] content below 20 wt%, both T_c and T_m slightly shift to lower temperatures, which decrease more prominently at higher IL content (P70, P60 and P50) as guided by the dotted line in Figs. 1(a) and 1(b) and also displayed in Fig. 1(c). This phenomenon on one hand is ascribed to the dilution effects[30, 31] of amorphous IL, and on the other hand might be attributed to the strong interactions between the PEO and IL[25]. Figure 1(d) shows the concentration dependence of the crystallinity X_c, which also exhibits decreasing trend, indicating that the presence of [BMIM][PF_6] as an amorphous component could suppress the crystallization of PEO. The X_c can be quantitatively calculated by using the equation of $X_c = \frac{\Delta H_m}{f_w \Delta H_m^0}$, where ΔH_m is the enthalpy of fusion from DSC measurement, f_w is the weight fraction of PEO in the mixtures and ΔH_m^0 is the enthalpy of fusion of 100% crystalline PEO (196.8 J/g)[32].

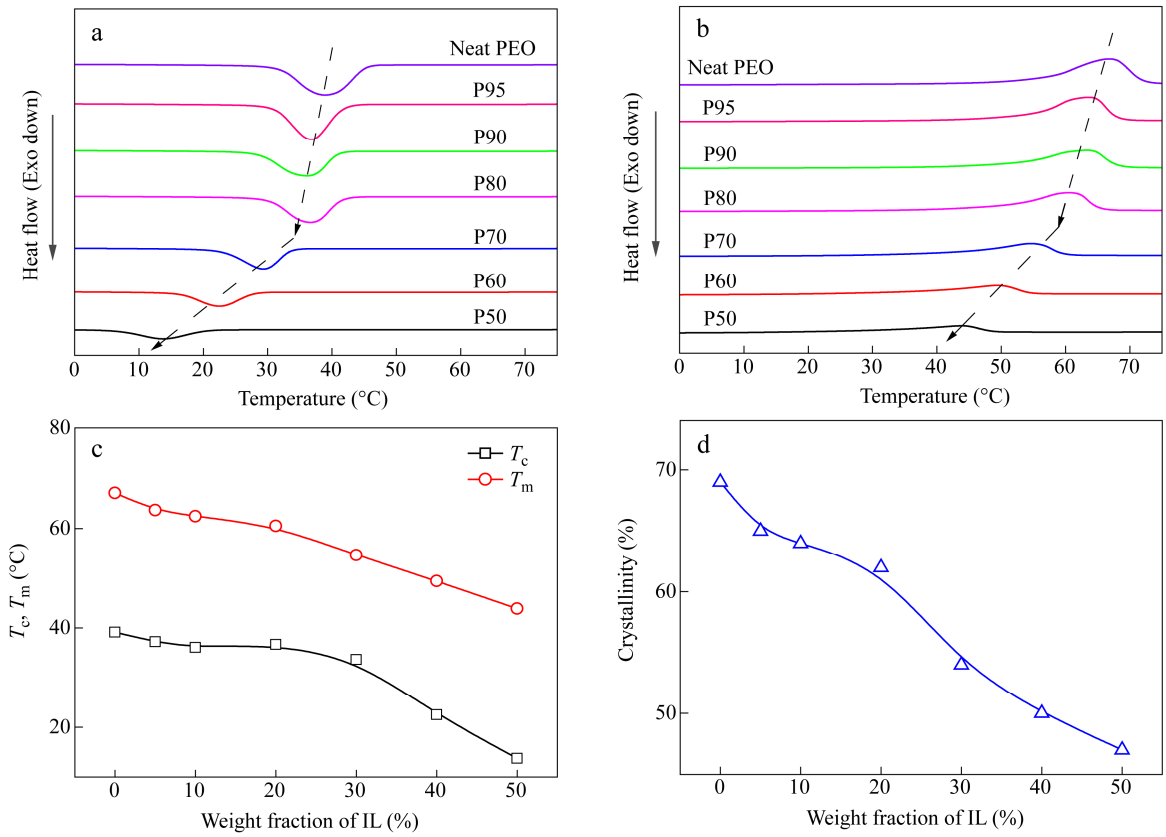


Fig. 1 DSC cooling (a) and heating (b) scan curves of PEO/[BMIM][PF_6] mixtures with different IL concentrations ranging from 0 wt% to 50 wt% and the concentration dependences of crystallization and melting temperatures T_c and T_m (c), and crystallinity X_c (d)

Isothermal Crystallization Behavior

The isothermal crystallization behaviors of P80, P90, P95 and neat PEO were studied at the isothermal crystallization temperatures of 43, 45, 47, and 49 °C. The Avrami equation is used to analyze the isothermal crystallization kinetics. It is assumed that the evolution of the relative crystallinity X_t with crystallization time t as

$$1 - X_t = \frac{\Delta H_{t=\infty} - \Delta H_t}{\Delta H_{t=\infty} - \Delta H_{t=0}} = \exp(-kt^n) \tag{1}$$

in which $\Delta H_{t=\infty}$ and ΔH_t are the crystallization enthalpies on complete crystallization and after time t, respectively, n is the Avrami exponent depending on the nature of nucleation and growth geometry of the crystals, and k is the crystallization rate constant involving both nucleation and growth rate parameters[33]. Taking the logarithm form, it can be expressed as:

$$\lg[-\ln(1 - X_t)] = \lg k + n \lg t \tag{2}$$

where k and n can be determined from the intercept and slope in the plot of $\lg[-\ln(1 - X_t)]$ versus $\lg t$. Then, the values of the half-time of crystallization $t_{1/2}$ can be calculated by the following Eq. (3), which is the time span required to achieve 50% of the final crystallinity of the samples.

$$t_{1/2} = (\ln 2/k)^{1/n} \tag{3}$$

Figure 2 selectively shows the changes of relative crystallinity X_t with the crystallization time t and the

corresponding Avrami plots for P95 sample at different crystallization temperatures and for neat PEO, P95, P90, and P80 samples at 49 °C. From Fig. 2(a), it can be seen that with increasing crystallization temperature from 43 °C to 49 °C, the induction time of crystallization for P95 becomes longer and the crystallization rate decreases, which is consistent with the previously reported results[28]. But the Avrami exponent n shown in Fig. 2(b) keeps almost constant with changing crystallization temperatures, as evidenced by the approximately same slope of Avrami plots. At a certain crystallization temperature, *i.e.* 49 °C in Fig. 2(c), the addition and increasing of [BMIM][PF_6] content significantly slow down the crystallization process of PEO. Similarly, the values of the Avrami exponent n are also independent of IL concentrations.

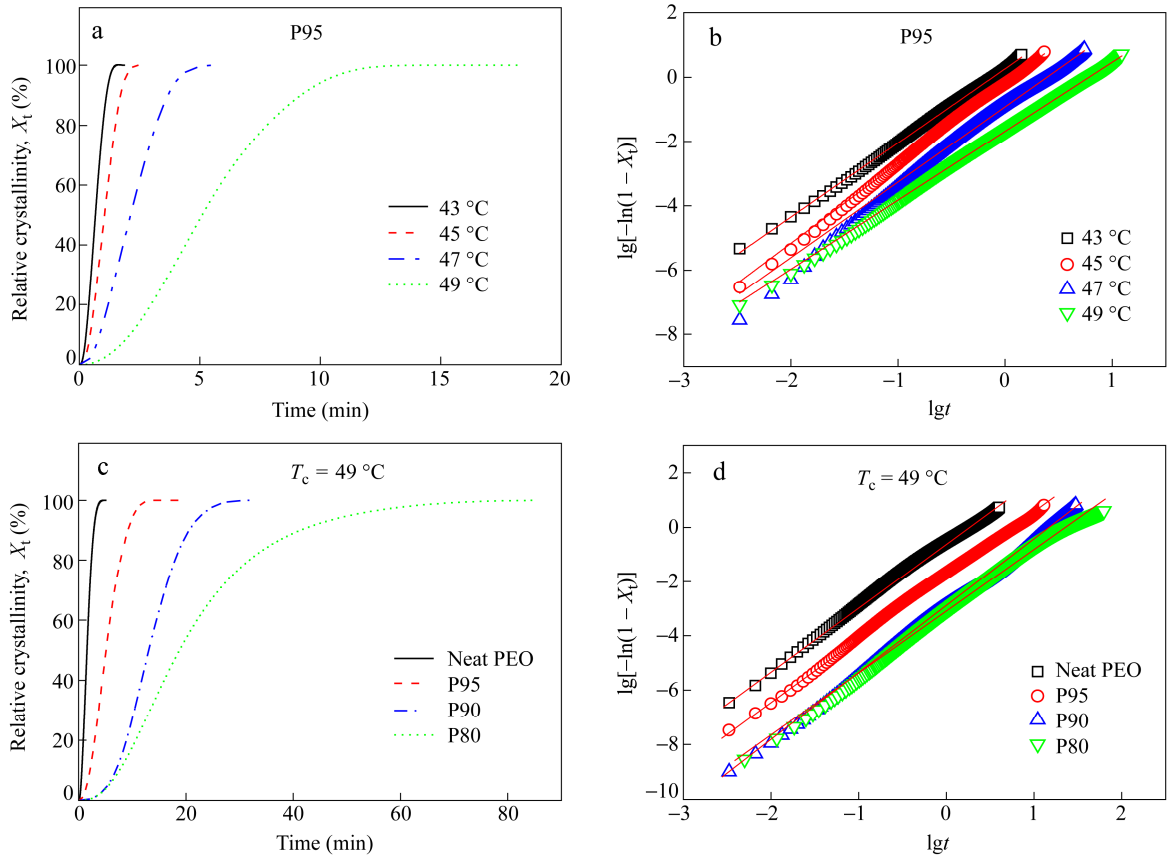


Fig. 2 Changes of relative crystallinity X_t with crystallization time t for P95 at different temperatures of 43, 45, 47, and 49 °C (a) and for P80, P90, P95 and neat PEO at 49 °C (c) with the corresponding Avrami plots (b) and (d)

To further compare the temperature and IL concentration dependences of the crystallization kinetics of PEO/[BMIM][PF_6] mixtures, Table 1 summarizes all the calculated crystallization kinetic parameters. One can see that the average values of n are all close to 2 for neat PEO, P95, P90, and P80 samples, indicating that the spherulite growth of PEO is two-dimensional with heterogeneous nucleation[34, 35]. In other words, the variation of crystallization temperature and the addition of [BMIM][PF_6] could not change the crystallization mechanism of PEO. For all the samples with different IL contents, the crystallization rate k decreases with increasing temperature due to the much lower degrees of undercooling ($\Delta T = T_m^0 - T_c$)[34]. Liu *et al.* have calculated the equilibrium melting point T_m^0 of PEO/[BMIM][PF_6] mixtures at various percentages, and found that the T_m^0 decreases almost linearly with increasing [BMIM][PF_6] content[25]. Therefore, the degrees of undercooling could decrease with both increasing crystallization temperature and IL concentration, which eventually leads to the increase of the half-time of crystallization $t_{1/2}$.

Table 1 Crystallization kinetic parameters of PEO/[BMIM][PF_6] mixtures

PEO/IL mixture	T_c (°C)	n	k (min^{-n})	$t_{1/2}$ (min)
100/0 (Neat PEO)	43	2.28	2.34	0.48
	45	2.28	1.55	0.70
	47	2.26	0.74	0.97
	49	2.18	0.26	1.57
95/5 (P95)	43	2.31	1.82	0.66
	45	2.49	0.65	1.03
	47	2.35	0.12	2.11
	49	2.22	0.02	4.94
90/10 (P90)	43	2.44	1.02	0.85
	45	2.45	0.22	1.60
	47	2.28	0.03	3.96
	49	2.59	0.001	9.98
80/20 (P80)	43	2.19	0.40	1.29
	45	2.19	0.08	2.68
	47	2.06	0.01	7.83
	49	1.97	0.001	19.46

Rheological time sweeps were also carried out to monitor the crystallization process at higher temperature. Rheology has been proven as a sensitive method to detect the gelation behavior at the earlier stage of crystallization or high temperature solidification[36–38]. Figure 3(a) shows the evolution of the storage and loss moduli G', G'' for neat PEO and PEO/[BMIM][PF_6] mixtures at 52 °C. Both G' and G'' increase with time for all samples, indicating the solidification process caused by the crystallization of PEO. During the induction period, there is a platform where $G' < G''$ can be observed because of the fully molten state of the samples[36]. With increasing IL content, consistent with the DSC results, the induction time becomes longer. This prolonged induction period indicates the much slower nucleation for the mixtures with higher IL concentration. After the induction period, G' and G'' both sharply increase caused by spherulite growth and filling process, during which $G' > G''$ occurs[39]. The crossover of G' and G'' reveals the crystallization induced critical gel formation[40, 41], which also increases remarkably with increasing IL concentration. At the late stage of crystallization, the second platform appears indicating the almost finished crystallization. The relative crystallinity X_t can also be derived from rheological parameters, *i.e.* G' or η^*[38]. Based on the below form:

$$X_t = \frac{G_t - G_0}{G_\infty - G_0} \tag{4}$$

where G_0, G_∞ and G_t are moduli before and after crystallization and at time t, the volume fractional X_t can be determined[39, 42]. The typical curves of X_t against crystallization time for pure PEO and its mixtures are shown in Fig. 3(b). Similar to the DSC results, the crystallization rate decreases apparently with the increase of [BMIM][PF_6] concentration. The calculated values of the halt-time of crystallization $t_{1/2}$ based on Eq. (3) for neat PEO, P95, P90 and P80 are 368, 1061, 3691, 5981 s, respectively, which further indicates that the addition and increasing [BMIM][PF_6] could significantly suppress the overall crystallization rate.

It is evident that $t_{1/2}$ becomes longer for PEO with the addition of [BMIM][PF_6] at a given temperature, indicating that the secondary amorphous component could remarkably slow down the crystallization of PEO. The concentration dependence of the overall crystallization rate ($V = 1/t_{1/2}$) of PEO at various crystallization temperatures is shown in Fig. 4. At all temperatures, the overall crystallization rate decreases exponentially with increasing IL concentration. As the temperature increases, the plot V versus weight fraction of IL shifts to lower values and the magnitude of this decreasing becomes smaller at higher temperatures, *i.e.* 49 and 52 °C. This indicates that the temperature plays a dominant role in determining the rate of the crystallization. However, the effect of IL concentration on the overall crystallization rate of PEO is somewhat complicated because of the dilution effect as well as the strong molecular interactions. It is worth noting that with a small amount of IL addition, *i.e.* P95, the crystallization rate declines dramatically at any given temperature, while with further

increasing IL content the magnitude of this decline becomes smaller especially at higher crystallization temperatures.

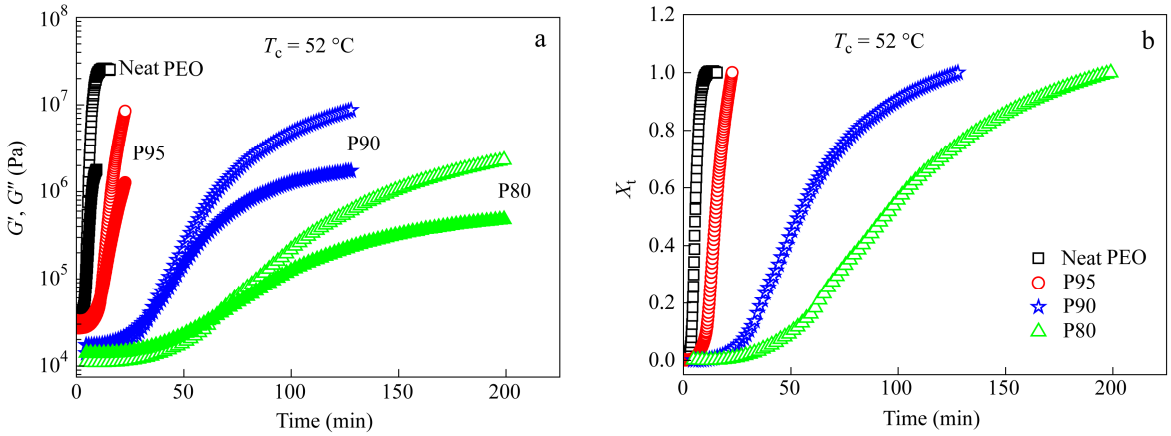


Fig. 3 Evolutions of storage modulus G' (open interior) and loss modulus G'' (solid interior), during time sweeps for neat PEO, P95, P90, P80 samples at 52 °C, respectively (a) and the corresponding time dependences of calculated crystallinity X_t (b)

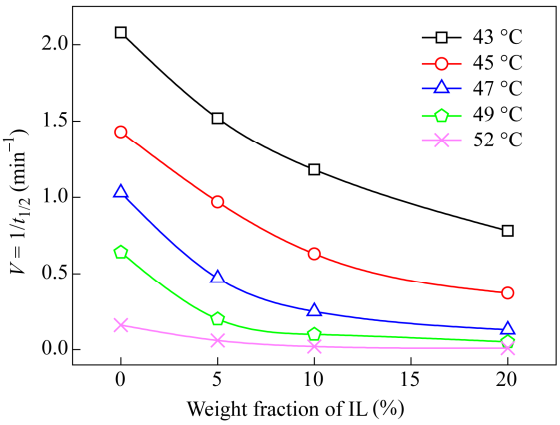


Fig. 4 Concentration dependences of the overall crystallization rate V for the PEO/[BMIM][PF_6] mixtures at different crystallization temperatures of 43, 45, 47, 49 and 52 °C V at 52 °C is measured by rheological method.

Nucleation and Spherulite Growth during Isothermal Crystallization

In order to further explore the effect of [BMIM][PF_6] on the crystallization of PEO, the nucleation and spherulite growth during isothermal crystallization process were observed by POM. Figure 5 shows the selected micrographs for pure PEO and PEO/[BMIM][PF_6] mixtures (P95, P90 and P80) crystallized at 49 °C. Typical spherulite structures can be observed for PEO and all the mixtures, but the spherulites become imperfect with the addition of [BMIM][PF_6]. The number of crystal nuclei shows the increase with increasing [BMIM][PF_6] concentration especially at higher IL content of P80, which might be due to the nucleation effect of [BMIM][PF_6] as heterogeneous nucleating agent[43, 44]. This seems controversy with the decrease of T_c, but we can tentatively interpret as follows. First, IL as heterogeneous nucleating agent could induce more nuclei as evidenced in Fig. 5 and meanwhile IL could also promote the mobility of PEO chains as a plasticizer[28]; these two factors lead to the enhanced crystallization. But on the other hand, the formation of strong hydrogen bonds between PEO and IL, which may restrict the mobility of PEO[45] as well as the dilution effects of IL, could conversely cause the retarded crystallization. The competitive effect might lead to lower T_c at higher IL concentration as shown in Fig. 1. Compared with the previous reports[26, 28], our study shows similar phenomena

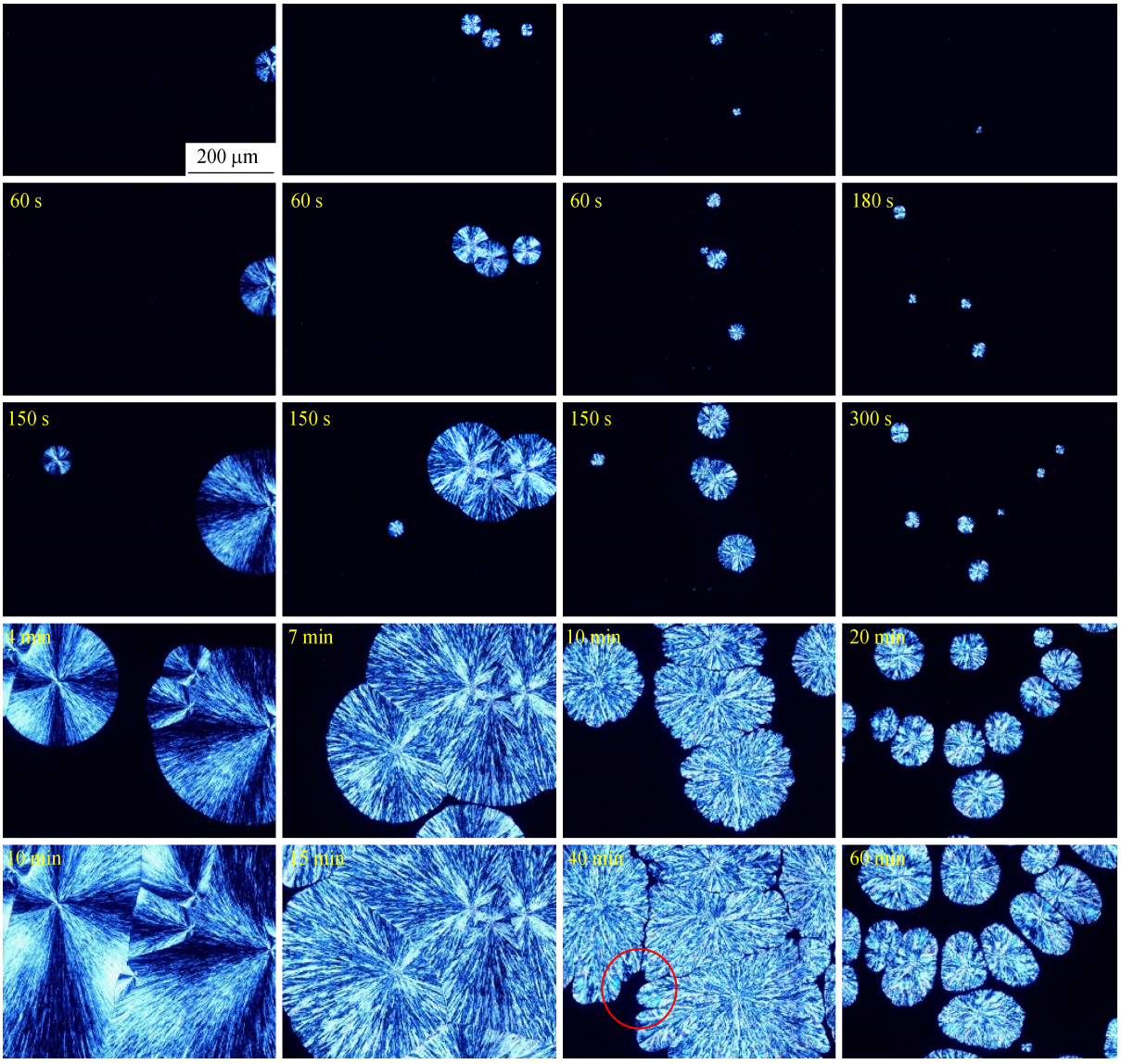


Fig. 5 Selected POM micrographs (50×) during the isothermal crystallization at 49 °C for pure PEO (a) and PEO/[BMIM][PF_6] mixtures: P95 (b), P90 (c), P80 (d)
The scale bar in panel (a) represents 200 μm and is applied to all other micrographs.

at the earlier stage of crystallization, but herein we paid more attention to the later stage spherulite growth. For pure PEO, the spherulites grow obviously larger than those of mixture samples, indicating the suppression effect of the [BMIM][PF_6] addition. Apparently at the later stages, the fine texture can be observed for different mixtures. With the addition of IL and increasing IL content, the irregular and coarser growth front of the spherulites can be observed for P95, P90 and P80 samples. The explanation of this irregular spherulite front of PEO/[BMIM][PF_6] mixtures lies in the fact that with the spherulite growing at higher temperature or concentrations, more IL molecules could be excluded from the crystal lamellar and tend to accumulate in the interfibrillar regions or at spherulite boundaries[46], which will inhibit the diffusion of PEO chains to pack into the spherulites. This inhibited diffusion of PEO as observed and discussed in other PEO/IL or blended systems might be on one hand due to the hydrogen bonded interactions between PEO and [BMIM][PF_6] and on the other

hand ascribed to the physical restriction at the growth front[25, 35, 47]. As marked by the red circle in Fig. 5(c), more obvious serrated appearance can be seen at the later stage of crystallization for P90 samples as interpreted by the diffusion restricted behavior. Interestingly, the flattening circular profile and the existent channels between spherulites for P80 could also be found. This phenomenon, like the one in another blended system[46], can be interpreted as that small molecular ILs impurities diffuse away radially in advance of the growing spherulites and accumulate at the growth front, which leads to the steadily reduced spherulite growth.

Based on the morphological evolution in Fig. 5, the spherulite radius R as functions of crystallization time t is illustrated in Fig. 6. At the earlier stage of crystallization in Fig. 6(a), the spherulite growth rate $G = dR/dt$ (the slope of the plot) decreases severely from 1.5 μm/s to 0.1 μm/s with increasing IL content, indicating the significantly inhibited crystallization. Figure 6(b) shows the plots of lg$R$ versus lg$t$ during the whole process of the spherulite growth. For samples P80 and P90, the linear to non-linear transition of the spherulite growth can be observed, that is, the spherulite radius changes from $R \propto t$ at shorter time to $R \propto t^{1/2}$ at longer time similar to other binary mixtures[12, 48]. This non-linear spherulite growth indicates a diffusion-controlled process[49].

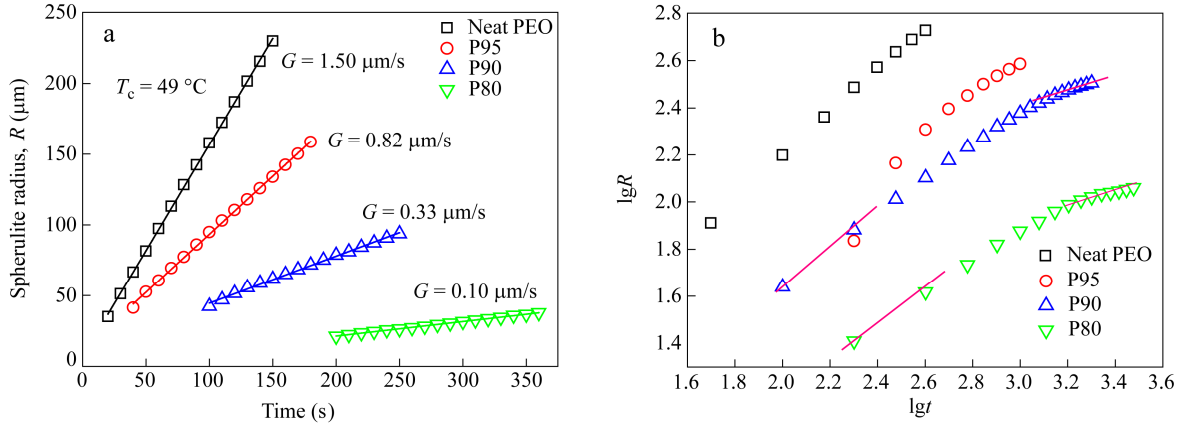


Fig. 6 Time dependences of spherulite radius at shorter crystallization time (a), and plots of lg$R$ versus lg$t$ during the whole spherulite growth (b) for pure PEO and PEO/[BMIM][PF_6] mixtures (P95, P90 and P80) at 49 °C

Spherulite growth is generally accompanied by the exclusion process of amorphous component, which is essentially dependent on the diffusivities of each component and governed by crystallization temperature, composition and molar mass, and even molecular interactions. Figure 7 shows the microstructure evolution of PEO spherulites for different mixtures at higher IL content under various crystallization temperatures. Figure 7(a) is the spherulitic pattern of P80 sample crystallized at 47 °C, in which a larger and more obvious jagged profile of the spherulites can be seen compared to those at 49 °C as illustrated in Fig. 5(d). Figures 7(b), 7(c) and 7(d) show the changes of spherulite morphology for P70, P60 and P50 mixtures crystallized at the respective temperatures of 41, 34, and 29 °C to ensure the sufficient spherulite growth rate. As shown in the micrographs, there is a transition from serrated to branched texture at the edge of the spherulite below P80. As IL content increases, the textures of the spherulite become coarser, and small angle branching could be seen clearly, that is, more sharp serrated profiles and irregular growth front appear at higher IL content above 20 wt%. This might be ascribed to the dilution effect as observed and proposed by Keith and Padden[46, 50, 51] of the IL in PEO matrix, which is a dominant factor governing the spherulite microstructure.

To further detect the finer morphological changes on the lamellar scale and for a better understanding of the crystal structure, wide angle X-ray diffraction (WAXD) and small angle X-ray scattering (SAXS) were conducted for pure PEO and PEO/[BMIM][PF_6] mixtures (P95, P90, P80). The prominent WAXD profiles for these samples are illustrated in Fig. 8; all samples exhibit two main peaks at 2θ of 19.3° and 23.4° corresponding to 120 and 112/004 reflections, respectively[32, 52, 53]. Compared with pure PEO, the IL addition does not alter crystal chain packing, and most likely, the PEO and IL do not cocrystallize consistent with the results of

Liu *et al*[25]. As the concentration of IL increases, the intensities of these diffraction peaks decrease slightly, in agreement with the DSC results. Besides the two well-defined diffraction peaks, for the PEO/IL samples, some broadening of the crystallographic peaks is observed, which might loosely be ascribed to the uncrystallized PEO and IL and the disorder of the crystal structure.

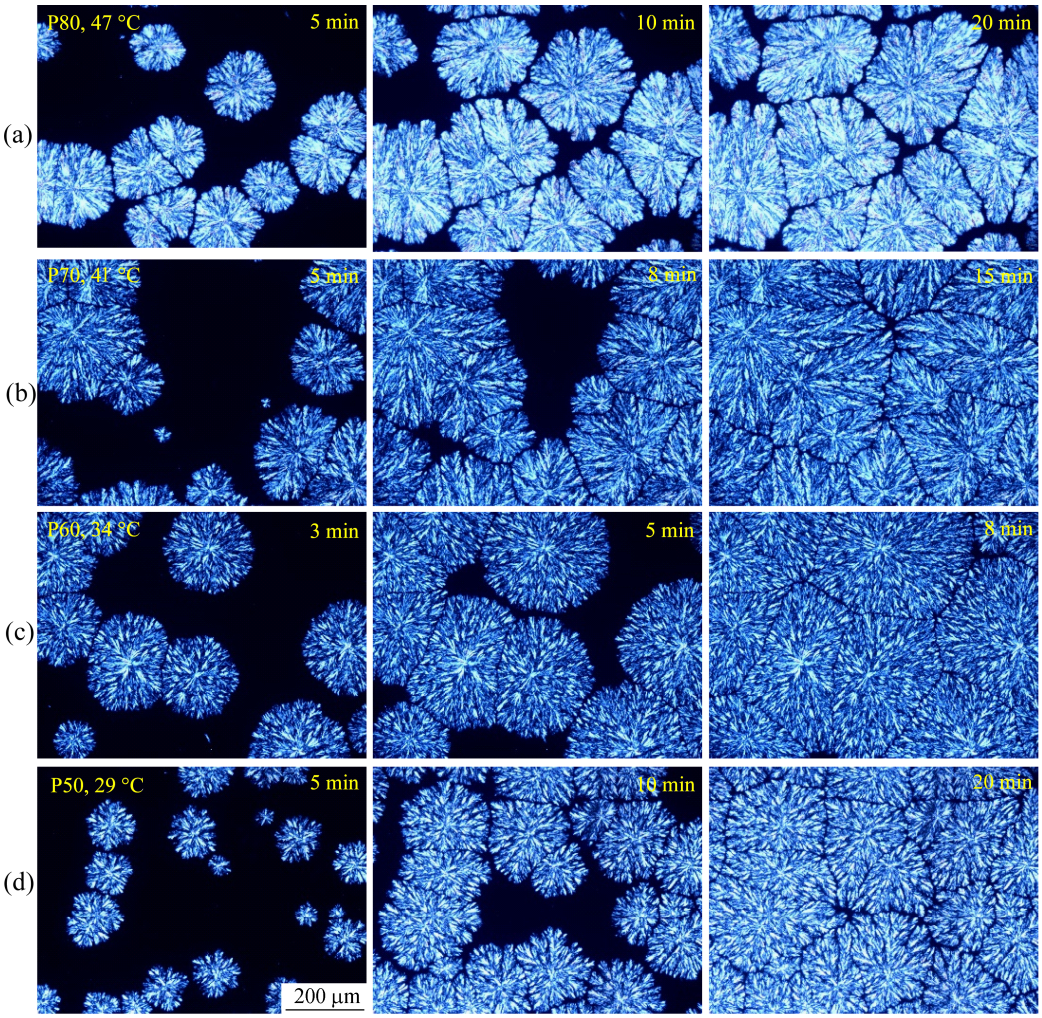


Fig. 7 Selected POM micrographs (50×) during isothermal crystallization for different PEO/[BMIM][PF_6] mixtures: sample P80 at 47 °C (a), sample P70 at 41 °C (b), sample P60 at 34 °C (c), sample P50 at 29 °C (d)
The scale bar in panel (d) represents 200 μm and is applied to all other micrographs.

Figure 9(a) shows the Lorentz-corrected SAXS intensity profiles (Iq^2 versus scattering momentum q ($q = \frac{4\pi}{\lambda}\sin\theta$, 2θ is scattering angle)) of samples crystallized for enough time at 49 °C. A typical scattering peak at q = 0.024 $Å^{-1}$ is observed for pure PEO similar to other research[54]. There is a large decrease in the peak intensity upon introducing 5 wt% [BMIM][PF_6] to PEO. As the IL concentration increases, the peak intensity further decreases, indicating that the addition of IL not only influences the formation of lamellar stack structure of PEO crystals but also causes the decrease of the crystallinity. Figure 9(c) shows the concentration dependence of the calculated long period L (determined using Bragg's law $L = 2\pi/q_{max}$, with q_{max} being the value at the SAXS peak) of the primary scattering peaks for PEO/[BMIM][PF_6] mixtures. The normalized one-dimensional correlation function is defined as:

$$g(r) = \int_0^\infty I(q)q^2 \cos(qr)\mathrm{d}q \Big/ \int_0^\infty I(q)q^2\mathrm{d}q \tag{5}$$

where the denominator or the normalizing factor is the scattering invariant (Q). The intensity at low q and high q regions was fitted by Guinier's law and Porod's law, respectively[57, 58]. The correlation functions deduced from

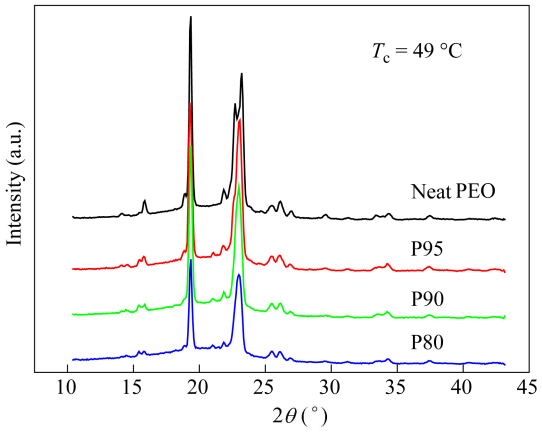


Fig. 8 WAXD profiles for neat PEO, samples P95, P90 and P80
All data were collected after the completion of the isothermal crystallization at T_c = 49 °C.

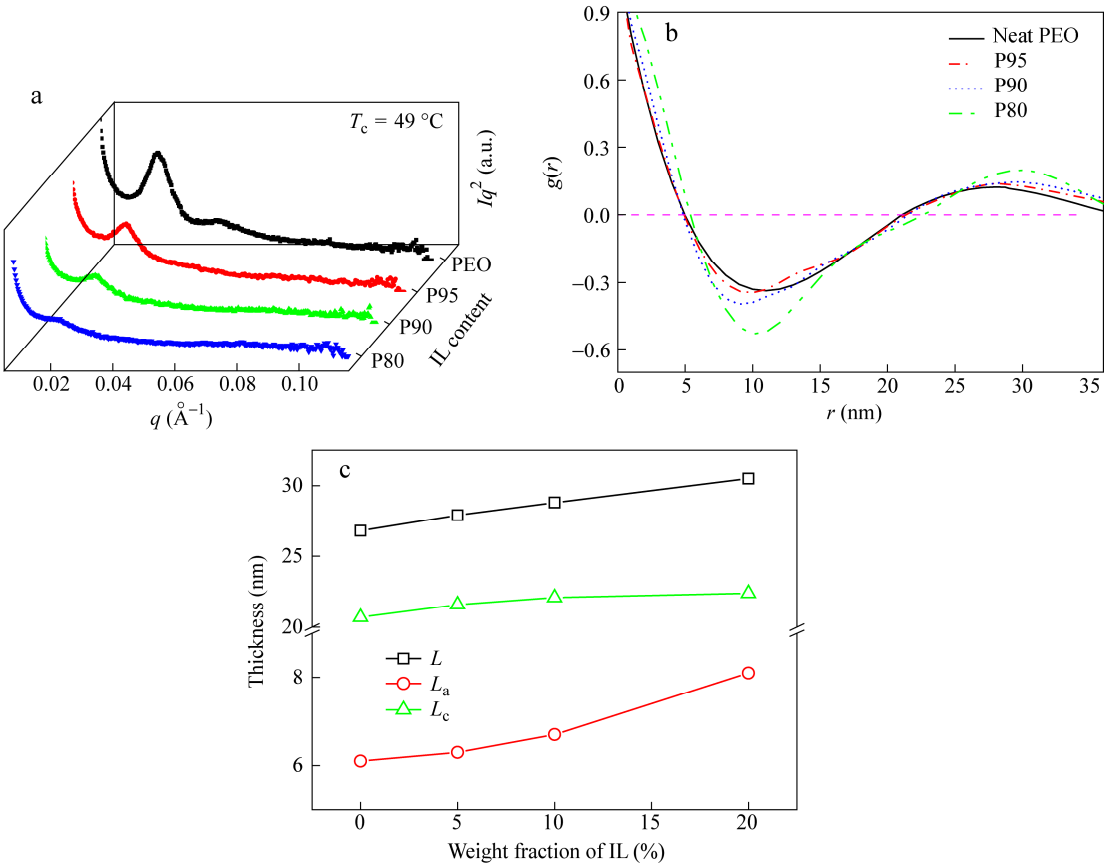


Fig. 9 Lorentz-corrected SAXS curves obtained at the isothermal crystallization temperature of 49 °C for neat PEO and PEO/[BMIM][PF_6] mixtures (a), the corresponding normalized correlation function (b), and the calculated long period L, thickness of crystal L_c and amorphous layer L_a versus IL weight fraction (c)

the scattering data, for neat PEO and PEO/IL mixtures are presented in Fig. 9(b). The thickness of the lamellar crystallites (L_c) (or the amorphous layer (L_a)) was obtained by the intersection between the slop of the triangle at $g(r) = 0$ and the horizontal line at the first minimum. The value of L_c should be larger than that of L_a due to the high crystallinity in neat PEO[54]. As shown in Fig. 9(c), with increasing [BMIM][PF_6] content, the long period L increases evidently from *ca.* 26 nm to 31 nm, with L_a slightly increasing while L_c almost keeping unchanged, that is, the increased L is mainly attributed to the increasing L_a. This can be interpreted as follows: with crystallization processing, more IL molecules within the lamellar stacks tend to be excluded and accumulated at the spherulite growth front, which will be trapped in the interlamellar regions when the IL content becomes larger and cause the increase of L_a. In other polymer blends systems[54–56] such as PEO/PMMA, this increased long period was directly related to the increasing thickness of the amorphous layer as more PMMA chains were introduced into the blend[54]. Thus, it is concluded that the addition and increase of the [BMIM][PF_6] concentration would cause the increase of the amorphous layer thickness, and consequently, result in the increase of the long period.

CONCLUSIONS

In this study, the crystallization kinetics and the spherulite morphological evolution have been investigated for miscible PEO/[BMIM][PF_6] mixtures. Crystallization of PEO is largely suppressed by [BMIM][PF_6] addition especially at higher IL concentrations above 20 wt%. Both the spherulite growth and the overall crystallization rate of PEO decrease with the increasing [BMIM][PF_6] content and crystallization temperature, however, the nearly constant Avrami exponent n close to 2 for all the samples including neat PEO and PEO/IL mixtures and their similar WAXD diffractions demonstrate the same crystallization mechanism without co-crystallization. Addition and increasing the [BMIM][PF_6] not only extend the induction time of crystallization despite more nuclei are induced, but also change the spherulite growth varying from $R \propto t$ to $R \propto t^{1/2}$. Rheology possesses higher sensitivity than DSC measurement on high temperature crystallization. The coarser surface and irregular growth front of the PEO spherulites at higher IL contents reveals the diffusion-controlled growth and the dilution effects. The increased long period with increasing IL content might be ascribed to the increased amorphous layer thickness. The influences of the molecular interactions between PEO and ILs on the crystallization kinetics will be presented in the next work.

REFERENCES

1 Armand, M. and Tarascon, J.M., Nature, 2008, 451: 652
2 Hallinan Jr., D.T. and Balsara, N.P., Annu. Rev. Mater. Res., 2013, 43: 503
3 Sun, C.N., Zawodzinski, T.A., Tenhaeff, W.E., Ren, F., Keum, J.K., Bi, S., Li, D., Ahn, S.K., Hong, K. and Rondinone, A.J., Phys. Chem. Chem. Phys., 2015, 17: 8266
4 Bi, S., Sun, C.N., Zawodzinski, T.A., Ren, F., Keum, J.K., Ahn, S.K., Li, D. and Chen, J., J. Polym. Sci., Part B: Polym. Phys., 2015, 53: 1450
5 Fenton, D., Parker, J. and Wright, P., Polymer, 1973, 14: 589
6 Berthier, C., Gorecki, W., Minier, M., Armand, M.B. and Chabagno, J.M., Solid State Ionics, 1983, 11: 91
7 Fullerton-Shirey, S.K. and Maranas, J.K., Macromolecules, 2009, 42: 2142
8 Cheng, S., Smith, D.M. and Li, C.Y., Macromolecules, 2014, 47: 3978
9 Gopinadhan, M., Majewski, P.W. and Osuji, C.O., Macromolecules, 2010, 43: 3286
10 Yue, R.J., Niu, Y.H., Wang, Z.G., Douglas, J.F., Zhu, X.Q. and Chen, E.Q., Polymer, 2009, 50: 1288
11 Young, W.S. and EppsIII, T.H., Macromolecules, 2009, 42: 2672
12 Wu, L.M., Lisowski, M., Talibuddin, S. and Runt, J., Macromolecules, 1999, 32: 1576
13 Talibuddin, S., Wu, L., Runt, J. and Lin, J.S., Macromolecules, 1996, 29: 7527
14 Lutkenhaus, J.L., Hrabak, K.D., McEnnis, K. and Hammond, P.T., J. Am. Chem. Soc., 2005, 127: 17228

15 Ye, Y.S., Rick, J. and Hwang, B.J., J. Mater. Chem. A, 2013, 1: 2719
16 Zhou, D., Zhou, R., Chen, C.X., Yee, W.A., Kong, J.H., Ding, G.Q. and Lu, X.H., J. Phys. Chem. B, 2013, 117: 7783
17 Mallakpour, S. and Rafiee, Z., J. Polym. Environ., 2011, 19: 485
18 Hough, W.L., Smiglak, M., Rodríguez, H., Swatloski, R.P., Spear, S.K., Daly, D.T., Pernak, J., Grisel, J.E., Carliss, R.D., Soutullo, M.D., Davis, J.H. and Rogers, R.D., New J. Chem., 2007, 31: 1429
19 Lewandowski, A. and Świderska-Mocek, A., J. Power Sources, 2009, 194: 601
20 de Souza, R.F., Padilha, J.C., Gonçalves, R.S. and Dupont, J., Electrochem. Commun., 2003, 5: 728
21 Wang, P., Zakeeruddin, S.M., Exnar, I. and Grätzel, M., Chem. Commun., 2002, 24: 2972
22 Lee, H.N. and Lodge, T.P., J. Phys. Chem. Lett., 2010, 1: 1962
23 Tsuda, R., Kodama, K., Ueki, T., Kokubo, H., Imabayashi, S. and Watanabe, M., Chem. Commun., 2008, 40: 4939
24 Xiao, Z.L., Larson, R.G., Chen, Y.L., Zhou, C.T., Niu, Y.H. and Li, G.X., Soft Matter, 2016, 12: 7613
25 Liu, F.Y., Lv, Y.X., Liu, J.J., Yan, Z.C., Zhang, B.Q., Zhang, J., He, J.S. and Liu, C.Y., Macromolecules, 2016, 49: 6106
26 Chaurasia, S.K., Singh, R.K. and Chandra, S., Solid State Ionics, 2014, 262: 790
27 Chaurasia, S.K., Kataria, S., Gupta, A.K., Verma, Y.L., Singh, V.K., Tripathi, A.K., Saroj, A.L. and Singh, R.K., RSC Adv., 2015, 5: 8263
28 Chaurasia, S.K., Singh, R.K. and Chandra, S., CrystEngComm, 2013, 15: 6022
29 Bai, Y.X., Wu, G.L., Zhang, Q., Zhang, C.F., Gu, J. and Sun, Y.P., J. Appl. Polym. Sci., 2015, DOI: 10.1002/app.42137
30 Shieh, Y.T., Liu, G.L., Hwang, K.C. and Chen, C.C., Polymer, 2005, 46: 10945
31 Bartczak, Z. and Martuscelli, E., Macromol. Chem. Phys., 1987, 188: 445
32 Rakkapao, N., Vao-soongnern, V., Masubuchi, Y. and Watanabe, H., Polymer, 2011, 52: 2618
33 Avrami, M., J. Chem. Phys., 1939, 7: 1103
34 Godovsky, Y.K. and Slonimsky, G.L., J. Polym. Sci., Part B: Polym. Phys., 1974, 12: 1053
35 Qiu, Z.B., Yan, C.Z., Lu, J.M. and Yang, W.T., Macromolecules, 2007, 40: 5047
36 Pogodina, N.V. and Winter, H.H., Macromolecules, 1998, 31: 8164
37 Niu, Y.H., Yang, L., Wang, H. and Wang, Z.G., Macromolecules, 2009, 42: 7623
38 Kelarakis, A., Mai, S.M., Booth, C. and Ryan, A.J., Polymer, 2005, 46: 2739
39 Khanna, Y.P., Macromolecules, 1993, 26: 3639
40 Liu, C.Y., Zhang, J., He, J.S. and Hu, G.H., Polymer, 2003, 44: 7529
41 Chambon, F., Petrovic, Z.S., MacKnight, W.J. and Winter, H.H., Macromolecules, 1986, 19: 2146
42 Boutahar, K., Carrot, C. and Guillet, J., Macromolecules, 1998, 31: 1921
43 Yi, Q.F., Wen, X.J., Dong, J.Y. and Han, C.C., Polymer, 2008, 49: 5053
44 Zhao, S.C., Cai, Z. and Xin, Z., Polymer, 2008, 49: 2745
45 Mondal, J., Choi, E. and Yethiraj, A., Macromolecules, 2013, 47: 438
46 Keith, H.D. and Padden, F.J., J. Appl. Phys., 1964, 35: 1270
47 Kestur, U.S. and Taylor, L.S., CrystEngComm, 2010, 12: 2390
48 Lee, C.H., Polymer, 1998, 39: 5197
49 Frank, F.C., Proc. R. Soc. London, 1950, A201: 586
50 Keith, H.D. and Padden, F.J., J. Appl. Phys., 1963, 34: 2409
51 Keith, H.D. and Padden, F.J., J. Appl. Phys., 1964, 35: 1286
52 Pulst, M., Samiullah, M.H., Baumeister, U., Prehm, M., Balko, J., Thurn-Albrecht, T., Busse, K., Golitsyn, Y., Reichert, D. and Kressler, J., Macromolecules, 2016, 49: 6609
53 Lai, C.Y., Hiltner, A., Baer, E. and Korley, L.T., ACS Appl. Mater. Interfaces, 2012, 4: 2218
54 Shi, W.C., Yang, J., Zhang, Y., Luo, J., Liang, Y.R. and Han, C.C., Macromolecules, 2012, 45: 941
55 Chen, H.L., Liu, H.H. and Lin, J., Macromolecules, 2000, 33: 4856
56 Chiu, H.J., Chen, H.L., Lin, T.L. and Lin, J., Macromolecules, 1999, 32: 4969
57 Verma, R., Marand, H. and Hsiao, B., Macromolecules, 1996, 29: 7767
58 Imai, M., Kaji, K. and Kanaya, T., Macromolecules, 1994, 27: 7103